Volume 3
Number 6
June 2024
Pages 1073-1248

Digital Discovery

rsc.li/digitaldiscovery

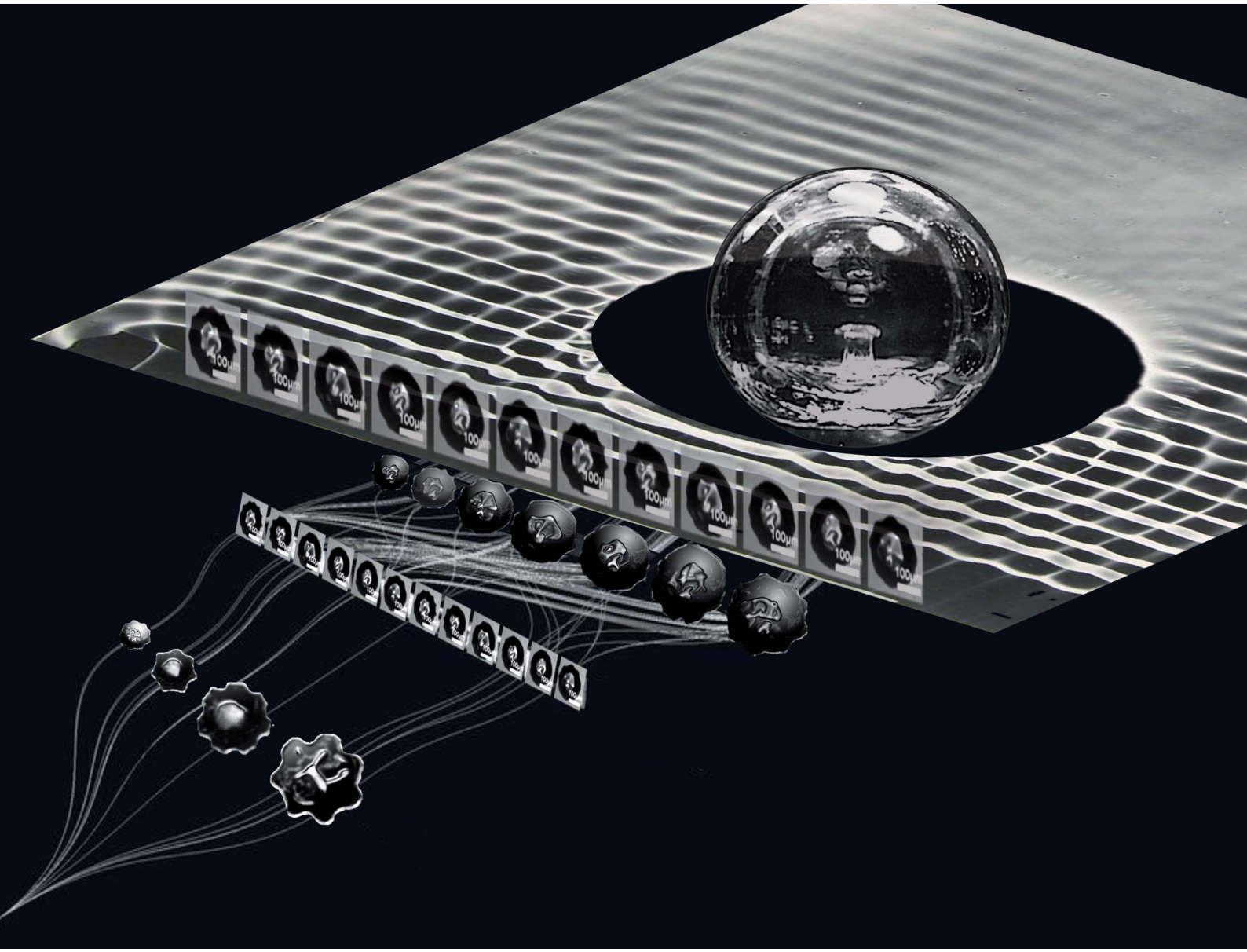

ISSN 2635-098X

ROYAL SOCIETY OF CHEMISTRY

PAPER

Michael Nosonovsky, Ekaterina V. Skorb *et al.*
Automatic image processing of cavitation bubbles to analyze the properties of petroleum products

Digital Discovery

ROYAL SOCIETY OF CHEMISTRY

PAPER

View Article Online
View Journal | View Issue

Cite this: *Digital Discovery*, 2024, **3**, 1101

Automatic image processing of cavitation bubbles to analyze the properties of petroleum products

Timur Aliev,[a] Ilya Korolev,[a] Olga Burdulenko,[a] Ekaterina Alchinova,[a] Anton Subbota,[a] Mikhail Yasnov,[a] Michael Nosonovsky *[ba] and Ekaterina V. Skorb *[a]

We have developed a new computer vision method of automatic image processing of cavitation bubbles to classify petroleum products with different octane numbers (ONs) using an artificial neural network (ANN). Ultrasonic irradiation induces cavitation bubbles, which exhibit growth, oscillations, and resonance shapes. Gasoline solutions may have different physical and chemical properties. While a precise understanding of how these properties impact bubble dynamics is challenging, training the ANN algorithm on bubble images allows classification of gasoline bubbles with different ON values. The integration of the ultrasonic cavitation method with computer vision and artificial intelligence techniques offers a promising way for real-time ON assessment in liquid flow.

Received 9th January 2024
Accepted 2nd April 2024

DOI: 10.1039/d4dd00003j

rsc.li/digitaldiscovery

1. Introduction

The real-time measurement and control of properties of viscous liquids in the fluid flow is important for many practical applications. Ultrasonic exposure of liquids including petroleum products can be used for this purpose. Cavitation with the formation of small bubbles is the common effect of the liquid's exposure to ultrasound.[1–6] Ultrasonic treatment also causes the dispersion of components in heterogeneous emulsions or suspensions and alters the colloidal stability.

By subjecting liquids to ultrasonic treatment and analyzing the response, it is possible to determine their characteristics. In addition to analyzing parameters such as soundwave propagation speed,[4,5] bubble size, and shape,[7–10] cavitation has been employed to estimate liquid's physical properties and composition.[7,11,12] Cavitation involves localized pressure changes that lead to the formation of bubbles composed of gas dissolved in a liquid and vapors of the solvent itself. For the evaluation of cavitation activity, the acoustic signal emitted by a sonotrode is transformed into an electric signal, which is then measured at a specific distance within the medium under investigation.

The behavior of cavitation bubbles is influenced by the environment surrounding them including the density and viscosity of the solution.[13–15] Cavitation processes have been utilized in various industries, such as shock freezing in the food industry,[16,17] chemical synthesis,[18–20] nanostructuring of materials,[21,22] and many others. Bubbles are also used in biomedical fields and drug delivery systems.[14] Their ability to collapse enables the targeted release of encapsulated drugs.[15] Understanding the cavitation process and accurately predicting the behavior of systems involving bubbles are crucial for the successful implementation of these applications.

In our previous study, we analyzed the composition of water–alcohol solutions based on the images of cavitation bubbles in these solutions.[7] The shape of the bubbles was contingent upon the concentration of the water–alcohol solution. This phenomenon stemmed from the disparity in liquid evaporation during ultrasound exposure; the lower quantity of solvent vapors within the solution had an impact on the bubble size and consequently, on its oscillation.

Cavitation bubbles undergo a certain evolution after their initial nucleation. When exposed to ultrasound, the size of bubbles oscillates due to the acoustic excitation causing compressive and tensile stress. During the compressive phase, bubbles shrink, while during the tensile phase, they expand for the amount that exceeds shrinking thus resulting in the growth of the average bubble radius. Following the oscillation stage, bubbles often destabilize and collapse or they decompose into parts. The bubble collapse is a very rapid process often leading to shock waves, very high local temperatures and high pressures, as well as to fluorescence.[7]

While behavior close to instability is difficult to predict by traditional deterministic methods, oscillating and collapsing bubbles can provide large amounts of datasets (*e.g.*, visual images), which make them an almost ideal object for artificial intelligence (AI) and machine learning (ML) analyses and searches for correlations in data.[23] ML also enables efficient real-time object tracking[24–27] which is significant for bubble behavior description. In our previous study, we used artificial neural

[a]*Infochemistry Scientific Center, ITMO University, 9 Lomonosov St., St. Petersburg, 191002, Russia. E-mail: skorb@itmo.ru*

[b]*Department of Mechanical Engineering, University of Wisconsin-Milwaukee, N Cramer St. 3200, Milwaukee, WI 53211, USA. E-mail: nosonovs@uwm.edu*

network (ANN) algorithms to analyze visual images of ultrasonic cavitation bubbles captured using a high-speed camera in water–alcohol solutions. The changes in oscillation modes of cavitation bubbles exhibit nonlinearity, which enables the application of artificial neural network (ANN) algorithms to analyze the distinct motion patterns of bubbles. The ANN was trained to determine the composition of these solutions based on the bubble images.[7]

In the present study, we will use a segmentation model with bubble properties automatically determined from visual images to further expand that approach and apply it to petroleum products. We will discuss the changes in cavitation activity and explore new applications for analyzing selected samples of gasoline with different octane numbers (ONs) (92, 95, and 98). Gasoline is a mixture of many different hydrocarbons, and its bulk consists of small C4–C12 hydrocarbons. The ON characterizes gasoline's resistance to detonation and it is measured relative to a mixture of 2,2,4-trimethylpentane and *n*-heptane. As different types of gasoline with different ONs have different densities and compositions, cavitation bubbles may have different evolution behavior. ANN algorithms will be utilized to recognize the ON of gasoline by training networks on images of bubbles captured in gasoline solutions with varying ONs. This approach holds potential for qualitative and quantitative analysis of flow systems involving petroleum products.

2. Materials and methods

2.1. Materials

Several samples of gasoline were selected for the study. Specifically, the samples included engine gasoline with the ON (RON) of 92, 95, and 98 (Shell® gas station), gasoline-solvent (Nefras C2-80/120) used in the rubber industry, and Shell FuelSave Unleaded 92, 95, and 98 – complex mixtures of hydrocarbons consisting of paraffins, cycloparaffins, aromatic and olefinic hydrocarbons with carbon numbers predominantly in the C4 to C12 range, with the specified densities of 0.735 g cm^{-3}, 0.750 g cm^{-3}, and 0.765 g cm^{-3} for RON 92, 95, and 98, respectively. Gasoline contained oxygenated hydrocarbons which include methyl tertiary butyl ether (MTBE) and other ethers as well as several additives at <0.1% v/v each.

2.2. Experimental methods

The ultrasonic generator UZG 55-22 (BSUIR, Belarus) was employed for the experiment. The generator had a nominal rated frequency of 22 kHz and a nominal maximum power of 100 W, which could be reduced to lower values. Ultrasonic oscillations were generated by the titanium sonotrode, which had a truncated cone shape with a disk (15 mm diameter, 2 mm thickness) at the edge. The sonotrode was positioned at an angle of 45° to the surface of a glass Petri dish filled with the liquid being studied. The immersion depth was adjusted to ensure that the entire disk was fully submerged in the sample liquid.

Note that while the property of interest is the ON which characterizes fuel's ability to detonate, even for a low ON ultrasonic cavitation bubbles cannot cause detonation due to their small size and energy.

To measure the cavitation activity, the portative cavitometer ICA-5D (BSUIR, Belarus) was used. To get the relevant data, the cavitometer's tip was submerged to the same level as the sonotrode disk at a distance of 4.5 cm from the disk. The cavitometer has standard software for the real-time cavitation activity registration and imaging. The total measurement time was 60 s for each measurement. The measurement was conducted for three values of ultrasonic generator specific power, 19 W cm^{-2} for the period 0–60 s, 38 W cm^{-2} for the period 61–120 s, and 67 W cm^{-2} for the period 121–180 s.

The cavitation bubbles were formed in the liquid samples as a result of the ultrasound treatment. The registration and imaging of the cavitation bubbles were conducted with the high-speed camera Phantom Miro C110, connected to the microscope Mikmed-6 (LOMO, Russia) with a 10× objective. The capturing frequency was 700 frames per second (fps) with a resolution of 768 × 768 pixels. The image set was automatically composed from the frame images as a single video file. The video file was edited with the application Phantom CV 3.3 to identify sections containing bubble formation, evolution and collapse for each sample.

2.3. Artificial neural network modeling

2.3.1. Software and hardware. The following software stack was used for the computational model: the Python 3.9 programming language, the Pip package manager, the PyTorch framework and add-on Lightning, and the Jupyter Notebook computational environment. Furthermore, additional Python modules were applied, such as Numpy for linear algebra computations, Matplotlib and Seaborn for visualization, Pandas for interaction with the dataset and data frame formation, and OpenCV for preparatory image processing. All versions of libraries for creating a virtual environment are described in the GitHub repository. A personal computer with processor AMD Ryzen Threadripper 3960X 24-core with a frequency of 3.8 GHz, the RAM volume of 64 GB, and the 2 GeForce RTX 3090 graphics card was used.

2.3.2. Collection, preprocessing, and curation of data. The database for training a segmentation model based on YOLOv8 (ref. 28) weights consisted of 600 images marked with masks. The basic confidence coefficient of the model was set to 0.3.

Preparation of the database for classification based on ResNet50 weights was carried out by decoding the obtained 27 experimental video files. So, the division into 3 classes was obtained. A total of 59 441 images were received. To sort out images without bubbles, a previously trained model based on YOLOv8 weights was used, and 42 020 images with bubbles were identified.

The data for the RON gasoline classification model were divided into data obtained from the segmentation model. There were frames divided into 4 classes: RON 92, 95, 98 frames and bubble-free frames. To carry out cross-validation verification and testing of the model, each class was divided into a training, validation, and test sample in a ratio of 80 : 10 : 10.

Image preprocessing included standardization and normalization in accordance with ResNet50 documentation. The data

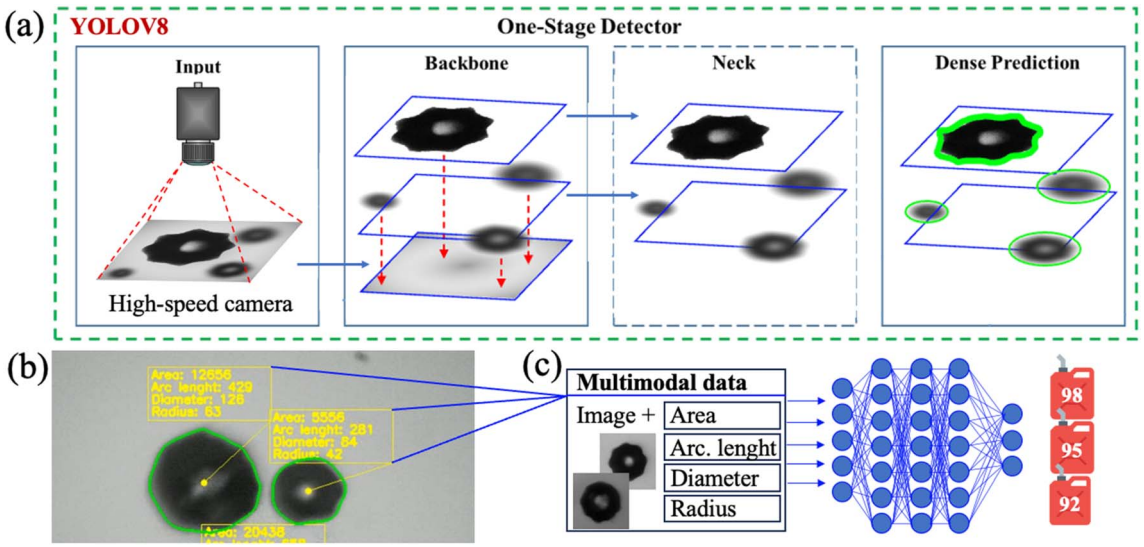

Fig. 1 The segmentation model of machine vision analysis showing (a) high-speed camera input, image isolation, necking, and density prediction to calculate, (b) the area, boundary length, diameter and radius to supply to the (c) ANN.

augmentation method, which includes rotations of images by random degrees and flips horizontally and vertically, was also used to avoid possible overfitting of the model.

2.3.3. Classification and segmentation models. For computer vision analysis, the ML segmentation model that allows selecting clusters of pixels related to an object (bubble) from images was used. The bubble contours were obtained (Fig. 1a) and data on the bubble image's area, boundary length, diameter and radius were obtained from the segmentation model (Fig. 1b). The obtained features (boundary length and radius) were used to train the classification model (Fig. 1c). The images were the first input set of the neural network, while the calculated parameters were used as the second input set. If there was no bubble, then the input was set to 0. The two input sets were combined.

3. Results

3.1. Observation and analysis of bubbles

Unlike for the water–alcohol solutions, which had been studied earlier,[7] in the present study we did not alter the concentration

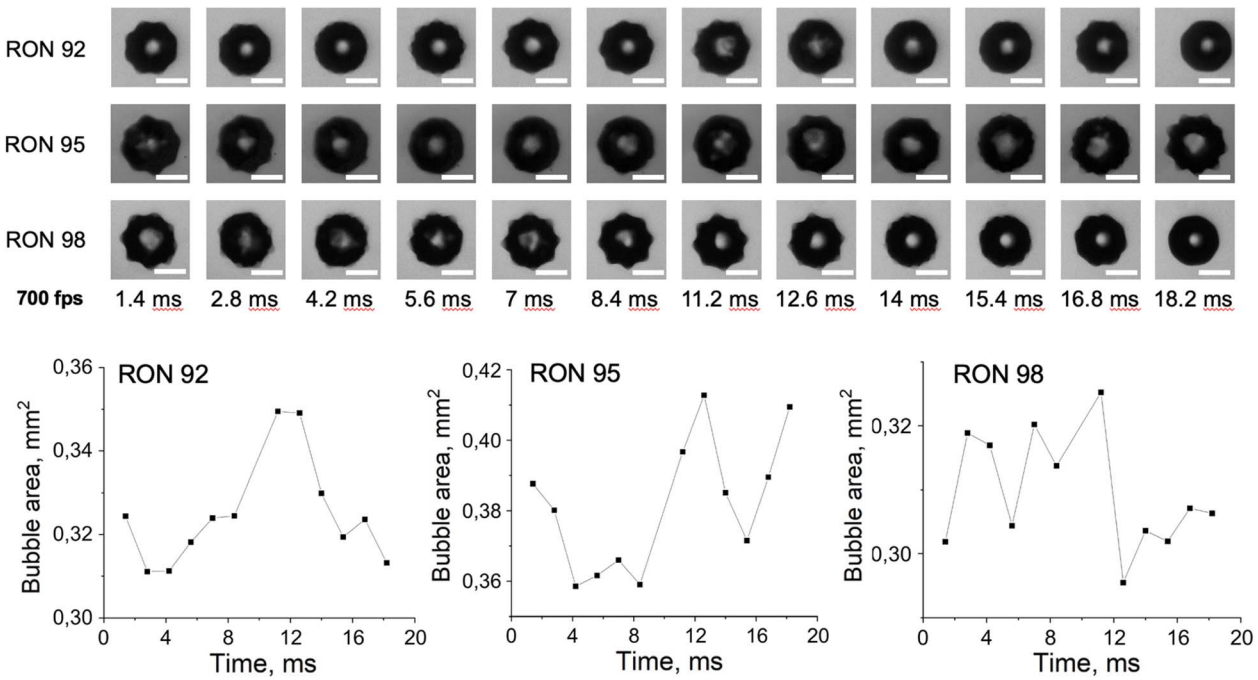

Fig. 2 Examples of bubble images at different time steps (scale length 500 μm) and variation of their area as obtained by the machine vision algorithm.

of gasoline. However, the composition and some physical properties of gasoline with different ONs tend to vary. This includes the specific density. The measurements were conducted on samples with the specified densities of 0.735 g cm^{-3}, 0.750 g cm^{-3}, and 0.765 g cm^{-3} for RON 92, 95, and 98, respectively. During the course of the experiment, we observed variations in the characteristic modes of oscillation of bubbles, which could be attributed to the different densities of the samples. Fig. 2 shows three examples of bubble evolution over time in different gasoline samples, as obtained by the ML algorithm. One can notice that the three bubbles demonstrate quite diverse behavior in terms of their evolution. Thus, while the maximum surface area is achieved at about 11–12 ms in all three samples, the RON92 and RON95 samples show a minimum surface area at 4 ms, while RON98 has a minimum at 13 ms. Moreover, RON92 has another minimum at 18 ms, while RON95 has a value close to the maximum at 18 ms. With a larger number of bubbles studied, more detailed trends can be determined. The total number of images studied constituted 59 441 frames.

For every frame of every video (total of 42 020 frames), a statistical analysis of cavitation bubbles was performed. No statistical correlation between bubble radii/area and ON was found. Consequently, an ML neural network model was applied.

3.2. Evaluating the effectiveness of a neural network model

The ML model was evaluated on a test sample that did not participate in the training. Fig. 3(a) presents the confusion matrix. The diagonal values of the confusion matrix indicate the fraction of correct prediction of the models. Thus, an average accuracy of 96% was obtained.

Fig. 3(b) shows the values of validation accuracy and the loss function of the number of epochs during training. There was no overfitting of the model, as validation accuracy increased, and losses decreased. It took 20 training epochs to train the model, the process took 3 hours. The Adam optimizer was used to find the minimum of the loss function. Its base learning rate was 10^{-3}. The scheduler ReduceLROnPlateau was also used to optimize the learning rate. CrossEntropyLoss was used as a loss function. The two heads of the model were combined using 4 linear layers. The total number of training parameters was 104 944.

The model was also evaluated with precision and recall metrics to assess the stability of the model (Fig. 3(c)).

To use the models, a web interface and API based on the FastAPI framework were coded. The resulting software allows deployment on a computing server for analyzing both already received videos and receiving data directly from a monitor for analyzing cavitation bubbles in real time. The code, model

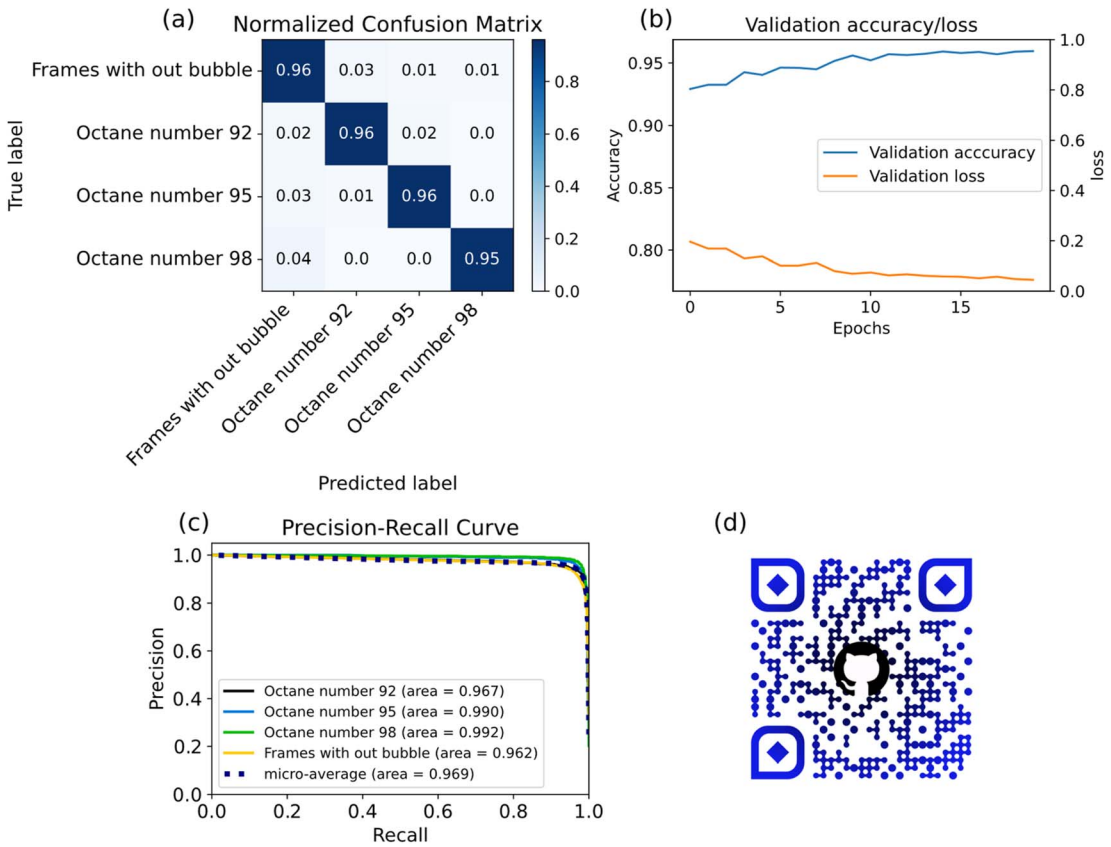

Fig. 3 (a) Confusion matrix representing the accuracy of each class of the classification model. (b) The dependency of validation accuracy and validation losses on the number of epochs during training. (c) Precision-recall curve demonstrating the stability of the model by evaluating the precision and recall metrics. (d) QR code with a link (https://github.com/ShockOfWave/itmo-collab) to the github repository containing the code, model weights, and data.

weights and data are presented in the repository on GitHub and Fig. 3(d) contains a QR code with a link to this repository.

4. Discussion

As gasoline consists of different hydrocarbons, those components which have light short molecules can easily evaporate. In the gaseous form, these components tend to dominate in cavitation bubbles and bubble behavior depends on their properties. As different types of gasoline have different chemical compositions, bubbles may behave differently inside samples with different ON values.

We found that bubble evolution is quite complex and it hardly can be accurately predicted for individual bubbles. However, the data collection and ML implementation allowed us to cluster the data belonging to different samples with significant confidence of 94%, 79% and 97%, from diagonal elements of the confusion matrix.

The high accuracy of the gasoline octane number classification based on the cavitation bubble image analysis of the implemented algorithm (Fig. 4) allows us to suppose that the shape of the bubbles correlates with the ON.

Dynamics of a spherical bubble is governed by the Rayleigh–Plesset equation.

$$R\frac{\mathrm{d}^2R}{\mathrm{d}t^2}+\frac{3}{2}\left(\frac{\mathrm{d}R}{\mathrm{d}t}\right)^2+\frac{4\nu}{R}\frac{\mathrm{d}R}{\mathrm{d}t}+\frac{2\gamma}{\rho R}+\frac{\Delta P}{\rho}=0 \quad (1)$$

where R is the radius, ρ is the liquid density, γ is the surface tension, ν is the kinematic viscosity, and ΔP is the pressure difference inside and outside the bubble. Consequently, the static equilibrium radius is $R_e = \frac{2\gamma}{\Delta P}$, as given by the Laplace equation. Nucleation of the bubble and its collapse are metastable processes so that the liquid and bubble states are separated by a small energetic barrier. Under the harmonically oscillating ultrasound, the pressure $\Delta P = \Delta P_0 + A\cos \Omega t$ reaches negative values when at minimum, so that the bubble passes through the tensile and compressive stages.[7]

At resonance, the destabilization occurs and the amplitude of an initially small perturbation of the spherical shape grows during periodic compression–expansion through a parametric instability. Consequently, the bubble undergoes shape oscillations and, natural frequencies of a spherical harmonic distortion of a droplet or bubble of order n (for $n > 1$) are given by the Rayleigh formula:

$$\omega_n{}^2 = (n-1)(n+1)(n+2)a \quad (2)$$

where $a = \frac{\gamma}{\rho {R_0}^3}$ (ref. 12) The lowest resonance frequency corresponds to $n = 2$, given that $n = 1$ corresponds to the displacement of the droplet as a whole. The value of the lowest resonance frequency is $\omega_2 = \sqrt{\frac{12\gamma}{\rho {R_0}^3}}$. Moreover, $n = 2$

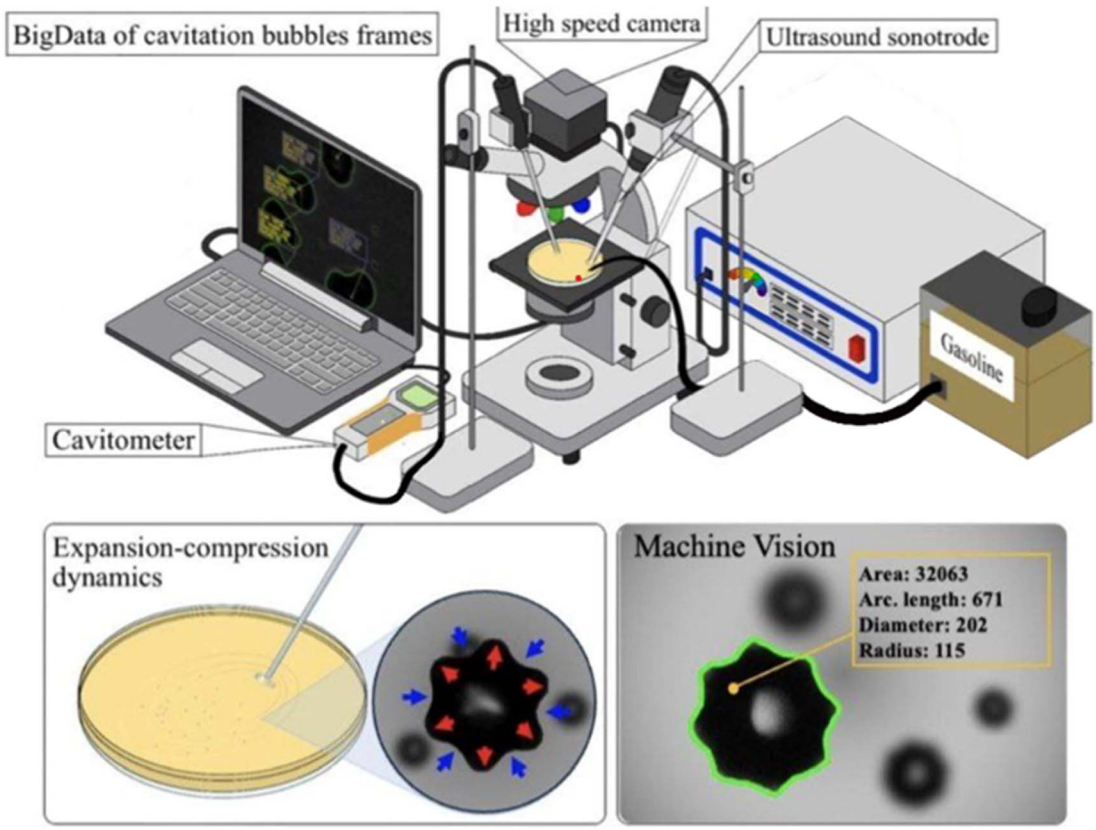

Fig. 4 Schematics of the experimental setup showing the liquid sample subjected to ultrasonic irradiation by the sonotrode causing cavitation. Bubble images captured with the high-speed camera and processed by software with an artificial neural network.

corresponds to the elliptical, $n = 3$ is the triangular, and $n = 4$ is the quadratic mode shape. For the frequency $f = \omega/2\pi$, the minimum resonance radius is

$$R_2 = \sqrt[3]{\frac{12\gamma}{\rho(2\pi f)^2}} \quad (3)$$

while mode n radius is

$$R_n = \sqrt[3]{\frac{(n-1)(n+1)(n+2)}{12}} R_2 \quad (4)$$

The density of the gasoline samples varies between 735 kg m^{-3} to 765 kg m^{-3}, while surface tension changes from 0.02 N m^{-1} to 0.03 N m^{-1}. Consequently, the ratio of $\frac{\gamma}{\rho}$ changes from 26×10^{-6} m^3 s^{-2} to 41×10^{-6} m^3 s^{-2}. At the ultrasound frequency of $f = 20$ kHz ($\omega = 125\,600$ rad s^{-1}), the value of $R_2 = \left(\frac{12\gamma}{\rho\omega^2}\right)^{\frac{1}{3}}$ is between $R_2 = 27$ μm and $R_2 = 31$ μm, which is consistent with the observations.

While the stability of the bubble can be estimated from various stability criteria, it is usually very difficult to predict how destabilization would occur. Therefore, statistical methods of analysis may be useful to establish insights.

5. Conclusions

Ultrasonic irradiation of gasoline (petrol) generates cavitation bubbles in the liquid. The properties of these bubbles and their evolution are influenced by the physico-chemical properties of the liquids. Since the bubbles manifest near critical and unstable behavior, it is very difficult to provide a criterion to distinguish bubbles in gasoline with different ONs. However, the large number of frames captured by a high-speed camera allowed us to train the ANN model to cluster data images and to distinguish between the three samples of petrol with different ONs. This shows potential for using high-speed camera images of cavitation bubbles to analyze in real time gasoline properties. Training the model on a greater dataset of cavitation bubble images for the samples provided by different producers will likely result in higher accuracy.

Data availability

The code and data used in this study are available in the GitHub repository at **https://github.com/ShockOfWave/itmo-collab**. This repository contains the source code used for the analysis, as well as the datasets utilized for training and testing the model. Researchers interested in replicating or extending this study can access the repository to review the code implementation and perform further analyses.

Author contributions

IK: visualization, methodology, writing – original draft; TA: software, project administration, visualization, writing – original draft; AS and MY: investigation, software; OB and EA: investigation, data curation, formal analysis; MN: supervision, writing – review & editing, EVS: project administration, supervision, conceptualization. All authors participated in writing and discussion of the manuscript.

Conflicts of interest

There are no conflicts to declare.

Acknowledgements

The research was carried out within the state assignment of the Ministry of Science and Higher Education of the Russian Federation (project No. FSER-2024-0003). Priority 2030 Program is acknowledged for infrastructural support. M. N. acknowledges sabbatical support from University of Wisconsin-Milwaukee.

References

1 M. R. Jalali and M. A. Sobati, Intensification of oxidative desulfurization of gas oil by ultrasound irradiation: Optimization using Box–Behnken design (BBD), *Appl. Therm. Eng.*, 2017, **111**, 1158–1170.
2 A. T. Hoang and V. D. Tran, Experimental analysis on the ultrasound-based mixing technique applied to ultra-low sulphur diesel and bio-oils, *Int. J. Adv. Sci. Eng. Inf. Techno.*, 2019, **9**(1), 307–313.
3 O. P. Stebeleva and A. V. Minakov, Application of Cavitation in Oil Processing: An Overview of Mechanisms and Results of Treatment, *ACS Omega*, 2021, **6**(47), 31411–31420.
4 M. M. Campos, L. E. Borges-da-Silva, D. A. Arantes, C. E. Teixeira, E. L. Bonaldi, G. Lambert-Torres, R. F. Ribeiro Junior, G. P. Krupa, W. C. Sant'Ana, L. E. L. Oliveira and R. G. de Paiva, An Ultrasonic-Capacitive System for Online Characterization of Fuel Oils in Thermal Power Plants, *Sensors*, 2021, **21**(23), 7979, DOI: **10.3390/s21237979**.
5 B. Nikolić, B. Kegl, S. D. Marković and M. S. Mitrović, Determining the speed of sound, density and bulk modulus of rapeseed oil, biodiesel and diesel fuel, *J. Therm. Sci.*, 2012, **16**, 505–514.
6 A. Shamseddini, D. Mowla and D. F. Esmaeilzadeh, Continuous treatment of petroleum products in a tailor-made flow-through sonoreactor, *J. Pet. Sci. Eng.*, 2019, **173**, 1149–1162, DOI: **10.1016/j.petrol.2018.10.0**.
7 I. Korolev, T. A. Aliev, T. Orlova, S. A. Ulasevich, M. Nosonovsky and E. V. Skorb, When bubbles are not spherical: artificial intelligence analysis of ultrasonic cavitation bubbles in solutions of varying concentrations, *J. Phys. Chem. B*, 2022, **126**(16), 3161–3169, DOI: **10.1021/acs.jpcb.2c00948**.
8 M. Ashokkumar, The characterization of acoustic cavitation bubbles – An overview, *Ultrason. Sonochem.*, 2011, **18**(4), 864–872, DOI: **10.1016/j.ultsonch.2010.11.016**.

9 S.-W. Ohl, E. Klaseboer and B. C. Khoo, Bubbles with shock waves and ultrasound: a review, *Interface Focus*, 2015, **5**(5), 20150019, DOI: **10.1098/rsfs.2015.0019**.

10 (*a*) M. Hauptmann, F. Frederickx, H. Struyf, P. Mertens, M. Heyns, S. De Gendt, C. Glorieux and S. Brems, Enhancement of cavitation activity and particle removal with pulsed high frequency ultrasound and supersaturation, *Ultrason. Sonochem.*, 2012, **20**, 69–76, DOI: **10.1016/j.ultsonch.2012.04.015**; (*b*) M. Guédra, S. Cleve, C. Mauger, P. Blanc-Benon and C. Inserra, Dynamics of nonspherical microbubble oscillations above instability threshold, *Phys. Rev. E*, 2017, **96**, 063104.

11 L. Yusuf, M. D. Symes and P. Prentice, Characterising the cavitation activity generated by an ultrasonic horn at varying tip-vibration amplitudes, *Ultrason. Sonochem.*, 2020, **70**, 105273, DOI: **10.1016/j.ultsonch.2020.105273**.

12 D. Baresch and V. Garbin, Acoustic trapping of microbubbles in complex environments and controlled payload release, *Proc. Natl. Acad. Sci.*, 2020, **117**(27), 15490–15496.

13 C. E. Udoh, V. Garbin and J. T. Cabral, Polymer nanocomposite capsules formed by droplet extraction: spontaneous stratification and tailored dissolution, *Soft Matter*, 2019, **15**(26), 5287–5295.

14 X. Shang and X. Huang, Investigation of the Dynamics of Cavitation Bubbles in a Microfluidic Channel with Actuations, *Micromachines*, 2022, **13**(2), 203.

15 S. Kentish, T. J. Wooster, M. Ashokkumar, S. Balachandran, R. Mawson and L. Simons, The use of ultrasonics for nanoemulsion preparation, *Innovative Food Sci. Emerging Technol.*, 2008, **9**(2), 170–175.

16 T. S. H. Leong, T. J. Wooster, S. E. Kentish and M. Ashokkumar, Minimising oil droplet size using ultrasonic emulsification, *Ultrason. Sonochem.*, 2009, **16**(6), 721–727.

17 M. Savchenko, M. Hurtado, M. T. Lopez-Lopez, G. Rus, L. Á. de Cienfuegos, J. Melchor and J. A. Gavira, Lysozyme crystallization in hydrogel media under ultrasound irradiation, *Ultrason. Sonochem.*, 2022, **88**, 106096.

18 Y. Attia and S. H. Abdel-Hafez, Nano Cu_2O catalyzed ultrasonic-assisted green synthesis of some seleno [2, 3-b] quinoline derivatives, *J. Organomet. Chem.*, 2022, **960**, 122245.

19 M. K. Schaefer, W. Raffelt, S. Zaremba and K. Drechsler, Ultrasonic mixing head for liquid composite molding: Process and material characteristics, *Polym. Compos.*, 2018, **39**(11), 3977–3985.

20 E. V. Skorb, D. G. Shchukin, H. Möhwald and D. V. Andreeva, Ultrasound-driven design of metal surface nanofoams, *Nanoscale*, 2010, **2**(5), 722–727, DOI: **10.1039/C0NR00074D**.

21 E. Kuvyrkov, N. Brezhneva, S. A. Ulasevich, E. V. Skorb and E. V. Sonochemical, nanostructuring of titanium for regulation of human mesenchymal stem cells behavior for implant development, *Ultrason. Sonochem.*, 2019, **52**, 437–445, DOI: **10.1016/j.ultsonch.2018.12.024**.

22 T. Hyeon, M. Fang and K. S. Suslick, Nanostructured molybdenum carbide: sonochemical synthesis and catalytic properties, *J. Am. Chem. Soc.*, 1996, **118**(23), 5492–5493.

23 T. Orlova, A. Piven, D. Darmoroz, T. Aliev, T. M. Tamer Abdel Razik, A. Boitsev, *et al.*, Machine learning for soft and liquid molecular materials, *Digital Discovery*, 2023, **2**, 298–315, DOI: **10.1039/d2dd00132b**.

24 H. Ren, W. Wang, W. Tang and R. Zhang, Machine eye for defects: Machine learning-based solution to identify and characterize topological defects in textured images of nematic materials, *Phys. Rev. Res.*, 2024, **6**, 013259, DOI: **10.1103/PhysRevResearch.6.013259**.

25 L. Sun, Y. Xu, Z. Rao, J. Chen, Z. Liu and N. Lu, YOLO Algorithm for Long-Term Tracking and Detection of Escherichia Coli at Different Depths of Microchannels Based on Microsphere Positioning Assistance, *Sensors*, 2022, **22**, 7454, DOI: **10.3390/s22197454**.

26 E. N. Minor, S. D. Howard, A. A. S. Green, M. A. Glaser, C. S. Park and N. A. Clark, End-to-end machine learning for experimental physics: using simulated data to train a neural network for object detection in video microscopy, *Soft Matter*, 2020, **16**, 1751–1759, DOI: **10.1039/c9sm01979k**.

27 Y. Mao, X. Zhou, W. Hu, W. Yang and Z. Cheng, Dynamic video recognition for cell-encapsulating microfluidic droplets, *The Analyst*, 2024, **149**, 2147–2160, DOI: **10.1039/d4an00022f**.

28 G. Jocher, A. Chaurasia and J. Qiu, *Ultralytics YOLO (Version 8.0.0) [Computer software]*, 2023, **https://github.com/ultralytics/ultralytics**.